JOURNAL OF AIRCRAFT
Vol. 40, No. 4, July–August 2003

Effect of Propeller Slipstream on Heat-Exchanger Installations at Low Reynolds Number

Ehab A. Elsaadawy*
McMaster University, Hamilton, Ontario, L8S 4L7, Canada
and
Colin P. Britcher†
Old Dominion University, Norfolk, Virginia 23529-0247

An experimental program whose objective was an improved understanding of the effects of intermittent turbulence shed by a propeller on the aerodynamics of heat-exchanger installations at low Reynolds numbers is reported. The primary application is unmanned high-altitude atmospheric science aircraft, forming part of Old Dominion University's effort to develop technology applicable to ERAST (Environmental Research Aircraft and Sensor Technology) class aircraft. Wind-tunnel results indicate that the propeller wake affects, but does not eliminate, laminar separation bubbles on a representative wing. Rather, the bubbles reform between wake passages, limiting the drag penalty caused by increased skin friction. Further, there appears to be a possibility of an enhancement in performance of suitably designed ducted heat-exchanger installations.

Nomenclature

AR	=	area ratio
b	=	plane at the fin of the two-dimensional inlet
C_P	=	pressure coefficient, $C_P = (P - P_\infty)/q_\infty$
c	=	chord length
E, e	=	mean and fluctuating parts of the output voltage of hot-wire (or hot-film) sensors
P	=	static pressure
q	=	dynamic head, $q = 0.5\rho V^2$
R	=	universal gas constant, $R = 8.315$ kJ/kmol . K
Re_c	=	chord Reynolds number
r	=	function of measured variables
U	=	overall uncertainty
u	=	streamwise, x, velocity component
u', v'	=	rms values of the fluctuations of the x and y velocity components; $u' = \sqrt{u^2}$, $v' = \sqrt{v^2}$
$\sqrt{(\overline{u^2})}/V_\infty\%$	=	turbulence intensity
V	=	mean velocity along the centerline of two-dimensional inlet
X	=	measured variable
x, y	=	streamwise distance and lateral distance (normal to surface), respectively
α	=	angle of attack, deg
ρ	=	air mass density

Subscripts

atm	=	atmospheric
i	=	inlet plane to the two-dimensional inlet
ref	=	reference value
s	=	static
∞	=	freestream

Introduction

INTEREST in uninhabited aerial vehicles (UAVs) is higher today than at any time since the end of World War II, spurred on by rapid advancements in the underlying technologies. Aiming to develop technologies that will lead to a new family of UAVs, the NASA Dryden Flight Research Center established the Environmental Research Aircraft and Sensor Technology (ERAST) program in 1994. Such UAVs could be used in upper-atmospheric science missions to help collect, identify, and monitor environmental data to assess global climate change. They could also carry telecommunications equipment to high altitudes, serving much like satellites for a fraction of the cost of putting a traditional satellite in space. There are many other applications of UAVs varying among military, commercial, and scientific arenas, as discussed in Ref. 1. These vehicles will fly at subsonic speeds, as low as 15 miles per hour (24 km/h) equivalent airspeed, at altitudes as high as 100,000 ft (30,480 m), and for continuous missions lasting as long as many days. According to an ERAST propulsion system selection study,[2] a propeller-driven aircraft powered by a turbocharged, spark ignition, gasoline engine operates at substantially lower thrust specific fuel consumption than a turbojet at typical design altitudes and speeds. This type of propulsion system employs multiple stages of turbocharging to reduce power loss with altitude by allowing the engine air intake manifold pressure to be maintained close to the sea-level value over the entire altitude range. Following each turbocharger stage, an intercooler removes some of the heat generated during compression. In addition to the cooling installation(s) required by the intercoolers, this power plant requires an oil cooler and an engine coolant radiator. The cooling installations are found to become extremely large if high altitudes are to be reached, leading to weight and possible airframe drag penalties. In response to this concern, many investigators have proposed methods of designing low-drag installations for the intercoolers or engine radiators.[3,4] Solar/electric aircraft cannot yet rival the speed or ruggedness of more conventional powered designs, and so cannot replace them in all applications.

Owing to the dramatic changes in atmospheric temperature and pressure through the mission profile of this class of UAVs, high aerodynamic performance must be achieved over an unusually wide range of Mach and Reynolds numbers. Mostly, a combination of low Reynolds number and high subsonic Mach number is the case.

Previous Research—Slipstream Effects

The effect of propeller slipstream on the aerodynamic characteristics of wings and the performance of ducted heat exchangers has received relatively little attention since the inception of the jet engine. Early investigations of the effects of propeller slipstreams on boundary-layer transition did not result in consistent conclusions. Young and Moris[5,6] concluded, through flight tests, that for smooth

Received 17 June 2002; revision received 2 April 2003; accepted for publication 5 April 2003. Copyright © 2003 by Ehab A. Elsaadawy and Colin P. Britcher. Published by the American Institute of Aeronautics and Astronautics, Inc., with permission. Copies of this paper may be made for personal or internal use, on condition that the copier pay the $10.00 per-copy fee to the Copyright Clearance Center, Inc., 222 Rosewood Drive, Danvers, MA 01923; include the code 0021-8669/03 $10.00 in correspondence with the CCC.

*Postdoctoral Fellow, Department of Chemical Engineering. Member AIAA.
†Professor, Aerospace Engineering Department. Associate Fellow AIAA.

wings with conventional sections the position of the transition point in the slipstream lay within the range 0.05c–0.1c. Hood and Gaydos[7] investigated the effect of a tractor propeller on the extent of laminar flow on the NACA 27-212 airfoil. The Reynolds numbers in their flight tests ranged from $3{\cdot}5 \times 10^6$ to $7{\cdot}6 \times 10^6$. They concluded that the tractor propeller caused the point of transition from laminar to turbulent flow to move from approximately midchord to a position near the leading edge; the accompanying increase in drag probably exceeded 100%. Wenzinger[8] made an investigation in the NACA 19-foot pressure tunnel of a 0.4-scale model of an existing pursuit airplane. From that investigation it was concluded that the propeller slipstream caused an increase in the drag of that portion of the low-drag (laminar flow) wing in the slipstream to a value about the same as that of a conventional wing without slipstream. Zalovcik[9] and Zalovcik and Skoog[10] describe in-flight boundary-layer and profile-drag characteristics of wing sections of a P-47D airplane utilizing NACA 230 series and NACA 66 laminar flow series wing sections. These wings were especially finished to give aerodynamically smooth surfaces having waviness of small magnitude. Their results show little effect of the slipstream on transition for the NACA 230 section; however, the test with NACA 66 series wing resulted in the transition point location moving forward from 50 to 20% chord, indicating a significant loss of laminar flow.

Time-dependent behavior, particularly at frequencies associated with propeller blade passage rate, was not measurable by the techniques commonly employed at that time. More recent flight experiments conducted using surface hot-film sensors in a laminar boundary layer in the propeller slipstream on the T-34C airplane[11] illustrated the existence of a cyclic time-dependent laminar boundary-layer behavior, resulting in convected turbulent packets between which the boundary layer appears to remain laminar. Such cyclic behavior suggests that the previous conclusions about the loss of laminar flow in propeller slipstream might be pessimistic.

Cooling System Installations

The typical geometry of a cooling installation comprises a cowling (fairing) around a heat exchanger. The fairing serves the obvious purpose of improving the aerodynamic shape presented to the external flow. It also regulates the airflow through the duct that it encloses, taking a definite mass flow from the external stream and supplying it to the heat-exchanger unit,[12] and most importantly, reduces the flow velocity ahead of the heat exchanger (i.e., diffusion). The flow ahead of the inlet is influenced very little by the particular shape of the duct behind, and the flow conditions near the exit are important only in so far as they affect the mass flow through the duct. The ratio of the mean velocity at the heat exchanger to the freestream velocity is the primary concern.

Diffusion, both internal and external to the inlet, is a function of inlet shape. Whereas internal diffusion is a function of the area change of the internal duct (and the internal boundary layer), external diffusion is a function of inlet opening area, the shape of the cowling, and the exit conditions. Internal diffusion will cause an adverse pressure gradient on the inside of the inlet lip, leading to concerns about boundary-layer separation. At high-altitude flight conditions the internal flow remains incompressible and is dominated by low-Reynolds-number effects, whereas the external flow is likely to be compressible. Internal flow separation would decrease the cooling efficiency of the heat exchanger, whereas external flow separation would increase the airframe drag. Reduction in drag will increase the aircraft's endurance, range, or ceiling and will reduce the amount of required heat dissipation.

Motivations and Objectives

There are many recent and demanding UAV applications, such as stratospheric science vehicles, operating at low Reynolds numbers and moderate Mach numbers, although the available experimental database on slipstream effects, especially at low Reynolds numbers, is very limited. The objectives of the present program therefore include exploration of the effect of the propeller wake on airfoil boundary layers and examination of the effect of the propeller wake turbulence on the performance of conventional heat exchangers, all in the low-Reynolds-number regime characteristic of ERAST-type aircraft.

Experimental Setup

Old Dominion University Low-Speed Wind Tunnel, Instrumentation and Propeller

The Old Dominion University (ODU) Low-Speed Wind Tunnel is an atmospheric pressure, closed-return, fan-driven type.[13] It has two tandem closed test sections $9 \times 8 \times 7$ ft and $3 \times 4 \times 8$ ft respectively, the latter being used for this work. To generate a slipstream, a 30-in.-diam. SYNTEC variable-pitch propeller, manufactured in Canada by NRG Research, Ltd., was installed into the test section in front of the model. The propeller freewheeled at the tunnel operating velocities, with different blade pitch angles set to alter the wake spacing.

Model pressure measurements were made using PSI Model 9010 pressure scanners with a range of 10 or 20 in. of water. Off-surface hot-wire measurements were taken with standard TSI probes, mostly Model 1210-T1.5 (true wires), or occasionally 1201-20 (fiber/films), connected to an IFA-100 anemometer, with an IFA-200 digitizer. Surface hot-film measurements were taken using DANTEC Model 55 films with the same anemometer and digitizer.

Models Used

Three models were used in the study, with results from two reported herein. A laminar flow airfoil provided fundamental information on the effect of the propeller wake on laminar and transitional boundary layers.[13,14] Next, a two-dimensional inlet airfoil, designed at ODU as low-drag cooling installation, provided an upper-surface flow with a separation bubble as the transition mechanism. Finally a two-dimensional inlet model provided an external flow with a large degree of diffusion.

Two-Dimensional Inlet-Airfoil Model

The two-dimensional inlet airfoil was intended to be used as a wing-root section of ERAST-class aircraft,[4] as shown in Fig. 1. Because the internal diverged channel, shown in Fig. 2, could have experienced massive flow separation without the correct flow resistance from a radiator core, it was decided to tackle internal and external flows separately. Hence, the internal slot was shaped as a channel, as shown in Figs. 3 and 4.

Constructed out of fiberglass, foam, and wood, the wind-tunnel model of the inlet airfoil was equipped with 37 static-pressure taps, whose locations, based on computational predictions, were concentrated in regions where laminar separation bubbles were predicted to exist. The taps were staggered at 10 deg relative to the streamwise direction. The model chord was 18 in. with a span of 24 in., determined by the end-plate design described in detail in Ref. 4. Figure 5 shows the two-dimensional inlet-airfoil mounted between the two end plates into the test section. The model was typically operated at a chord Reynolds number of 5×10^5.

The end plates served as a support for a flush-mounted traversing system, based on opposing Unislide™ assemblies, used to position a pitot-static wake rake. The rake consisted of five pitot-static probes distributed in the spanwise direction of the model mounted to a streamlined, steel strut. This custom rake design enabled the simultaneous wake survey of five spanwise stations; therefore, it was unlikely that any spanwise variation in drag could be temporal in nature. Following contemporary practice in testing of two-dimensional low-Reynolds-number airfoils, the probes were unevenly spaced to avoid matching the wavelength of any periodic spanwise variation.

Two-Dimensional Inlet Model

The two-dimensional inlet model has a 12-deg internal angle (2δ), 0.14c maximum thickness, and 0.3c inlet opening area, as seen in Fig. 6. To begin the design process, a Selig 1210 airfoil was selected from a group of recently developed high-lift, low-Reynolds-number airfoils as a primary airfoil. An inverse design approach was then utilized wherein the original upper-surface-pressure distribution was

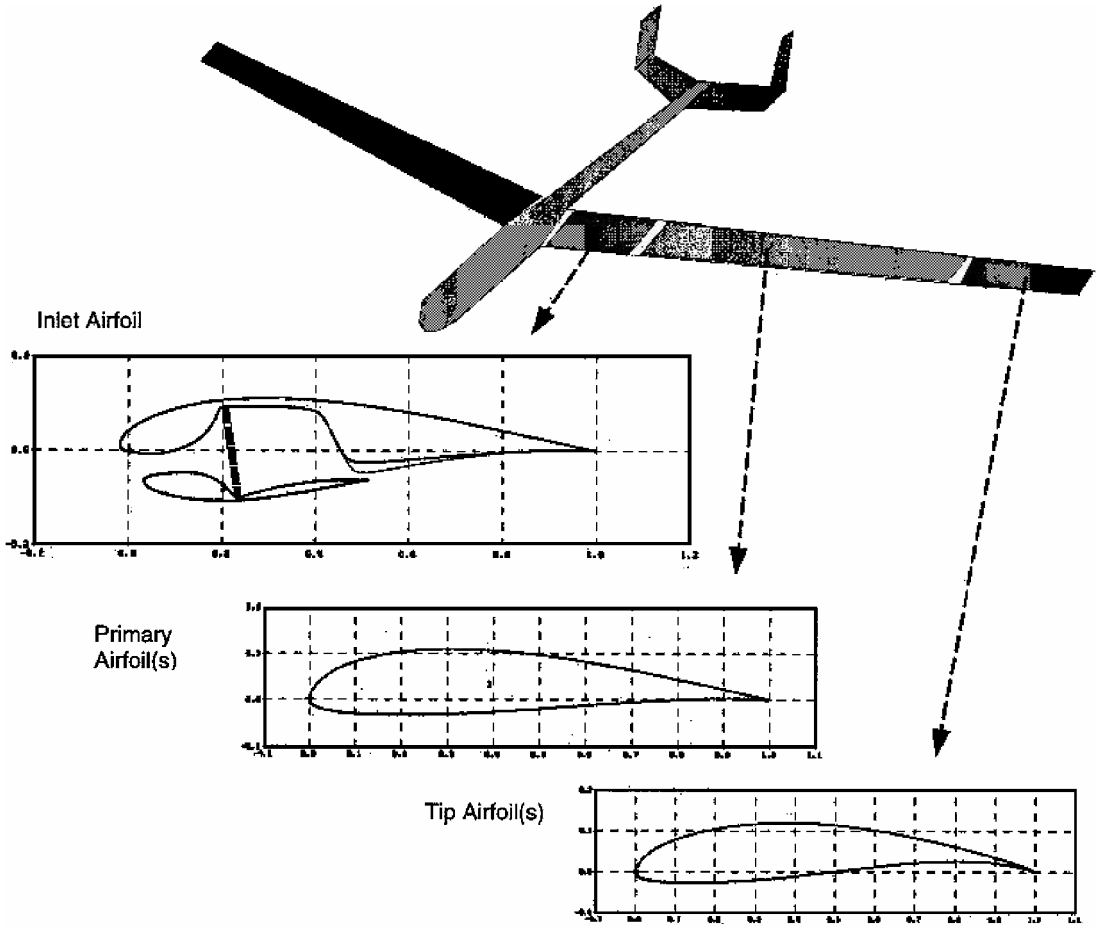

Fig. 1 Two-dimensional inlet-airfoil as a root airfoil.

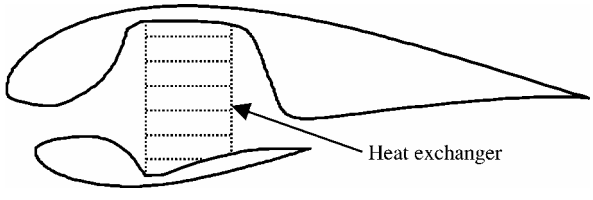

Fig. 2 Cross section of the two-dimensional inlet-airfoil, as designed.

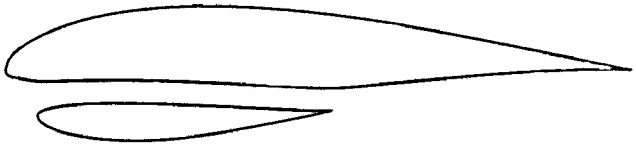

Fig. 3 Cross section of the two-dimensional inlet-airfoil, as built.

Fig. 4 Photograph of the two-dimensional inlet-airfoil model.

preserved, while meeting inlet velocity ratio and external diffusion requirements. The inner surfaces were made flat.[15]

The wind-tunnel model was constructed out of wood, foam, and fiberglass with an 18-in. chord and 36-in. span. The model was equipped with seven pressure taps on one element, five on the outer surface and two on the inner surface. The taps on the outer surface were distributed across the middle third of the model span and staggered at an angle to the streamwise direction. A thin "fin" was installed in a location somewhat representative of an internal heat exchanger, but used primarily as a mounting surface for hot-film sensors, which then measured in the developing fin boundary layer.

Results and Discussions

Two-Dimensional Inlet-Airfoil—Wake Effect on Laminar Bubble

Measurements on the two-dimensional inlet-airfoil are concerned mainly with the effect of the propeller slipstream on both the separation bubble and the transition process. At a chord Reynolds number of 5×10^5, the pressure distributions on the model outer surfaces show that the laminar separation bubble, formed on the airfoil upper surface, exhibits its characteristic "flat spot" in the pressure distribution, as can be seen in Fig. 7 (e.g., at about 0.25c at 6-deg angle of attack). With the propeller wake introduced, this feature disappears, as shown in Fig. 8. This could be interpreted as evidence of transition occurring prior to the bubble location, thereby eliminating the bubble, but this is found to be an incorrect conclusion. Rather, velocity

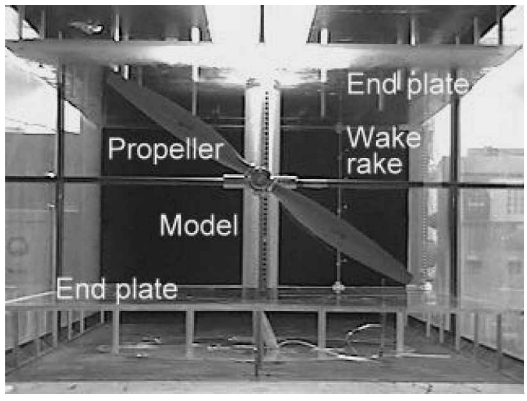

Fig. 5 Two-dimensional inlet-airfoil, end plates, and propeller installed in the wind tunnel.

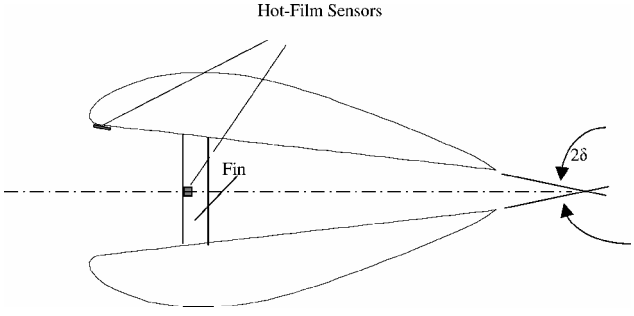

Fig. 6 Cross section of the two-dimensional inlet.

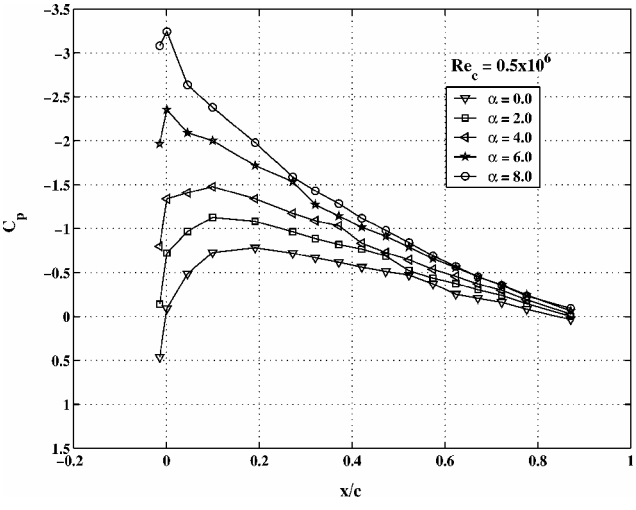

Fig. 7 Pressure distributions on the upper surface of the two-dimensional inlet-airfoil—no propeller.

profile measurements[14] suggest that the bubble appears surprisingly stable, and the pressure distribution of Fig. 8 is the result of temporal and spatial averaging as the propeller wake sweeps through the bubble.

Laminar, transitional, and turbulent flow boundary-layer states can be determined from the fluctuating part of the hot-film signals.[16] In the current work the ratio of the rms voltage to the mean voltage across the anemometer bridge was obtained for a chordwise array of six hot films, located at 0.3, 0.4, 0.5, 0.6, 0.65, and 0.7c. For both cases (with and without propeller) the data indicate three distinct regions where the boundary layer is first laminar, then transitional, and finally fully turbulent. The beginning of the transitional region (between the beginning and end of the transition process) is marked by a sudden rise in the normalized voltage. In the transition region the normalized voltage reaches a peak then rapidly decreases to a

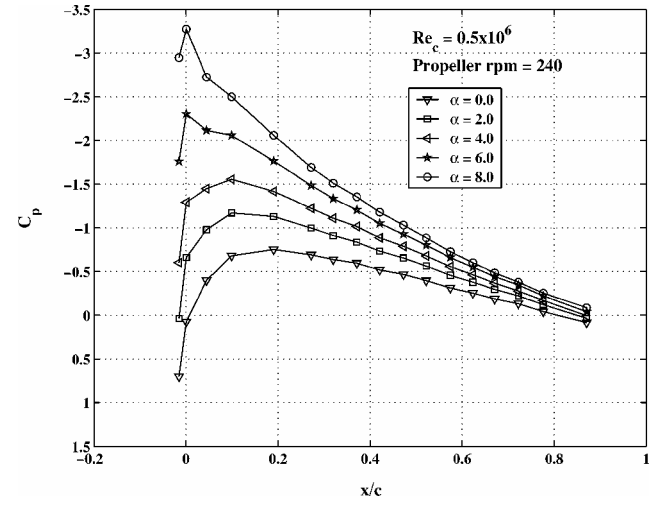

Fig. 8 Pressure distributions on the upper surface of the two-dimensional inlet-airfoil—with propeller at 240 rpm.

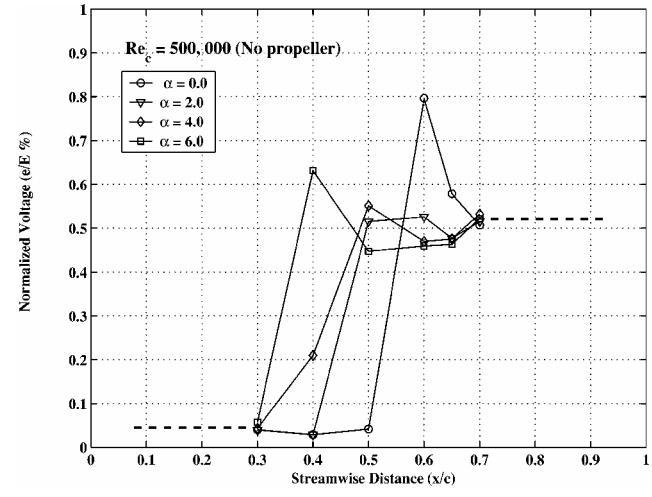

Fig. 9 Normalized hot-film voltages at different streamwise locations—no propeller.

point where the voltage again has a nearly constant value, indicating the end of transition.[17] In the case where no propeller slipstream is introduced, Fig. 9 shows that the normalized voltage for the laminar boundary layer upstream of the beginning of transition has a value of about 0.04 at all angles of attack while the normalized voltage for the fully turbulent boundary layer downstream of the end of transition has a value between about 0.45 to 0.5. As the angle of attack increases from 0.0 to 6.0 deg, the location of the beginning of transition correspondingly moves forward from 50 to 30% of chord. This forward movement of the beginning of transition is expected, based on the pressure distributions shown in Fig. 7.

Uniformly distributing the propeller periodic turbulence along the whole wake passage cycle and computing the corresponding mean and rms values, one can see from Fig. 10 that the start of transition moved upstream, and consequently the corresponding peak, at each angle of attack, also moved about 10%c upstream. The normalized voltage for the fully turbulent boundary layer downstream of the end of transition has increased to a value between about 0.6 to 0.8 instead of 0.45 to 0.5 earlier. Now, with the existence of the propeller slipstream, transition has at least intermittently moved forward from the location of the separated shear layer. In other words, the transition mechanism has changed, at least intermittently, from that associated with a laminar separation bubble, to a classical transition process more commonly associated with increasing the Reynolds number. Further details can be found in Ref. 14.

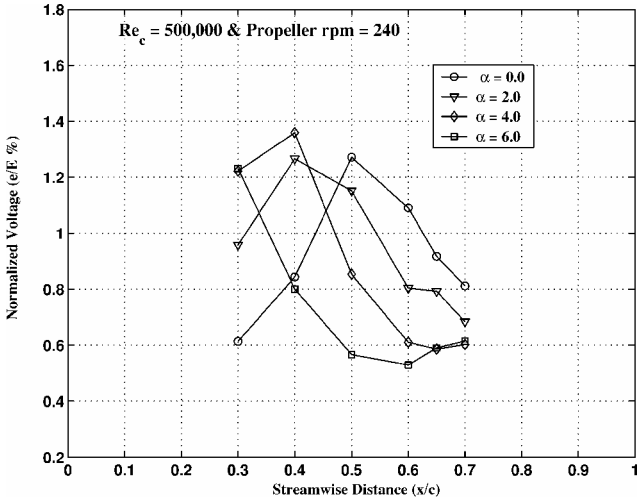

Fig. 10 Normalized hot-film voltages at different streamwise locations—with propeller at 240 rpm.

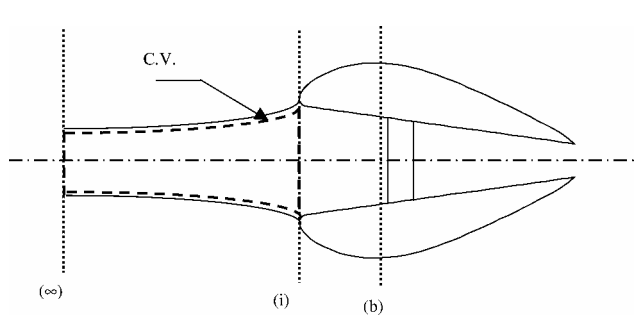

Fig. 11 Stream-tube analysis of turbulent velocity fluctuations.

Two-Dimensional Inlet—Wake Effect on Ducted Heat Exchanger

In this section the emphasis is on the effect of the propeller slipstream on the flow diffusion of a two-dimensional inlet. Prandtl was one of the first to consider turbulent velocity fluctuations caused by vortex filaments aligned with and normal to the flow in a wind-tunnel contraction or diffuser. Considering the stream tube [control volume (C.V.)] shown in Fig. 11, the vortex filaments aligned with the axis are shortened, producing a decrease in v' and w', whereas those normal to the axis are stretched, producing an increase in u' in the stream tube.[18] Application of Kelvin's Circulation Theorem gives

$$u_i'/u_\infty' = AR, \qquad v_i'/v_\infty' = w_i'/w_\infty' = 1/\sqrt{AR} \tag{1}$$

Because $(V_i/V_\infty) = AR$, then the relative turbulence intensities become

$$(u_i'/V_i) = AR^2 * (u_\infty'/V_\infty), \qquad (v_i'/V_i) = \sqrt{AR} * (v_\infty'/V_\infty) \tag{2}$$

This theory has a number of limitations, one of them being that random mixing caused by turbulence suppresses the preferential stretching or squashing of vortex filaments by exchange of energy between degrees of freedom. Thus, for the C.V. and according to the theory, the longitudinal turbulence intensity of the flow should grow while that of the lateral turbulence should vary little. On the other hand, inside the two-dimensional inlet the opposite should happen. However, the measurements shown in Fig. 12 show that, with no propeller slipstream, the turbulence intensity is more or less constant all of the way along the stream tube until the entrance plane i of the two-dimensional inlet and then decreases through the contracting part until plane (b), see Fig. 11. Although the decrease of the turbulence intensity in the contracting part of the inlet is consistent with the theory just presented, constant turbulence intensity along the stream tube, which is divergent, seems to be incompatible with

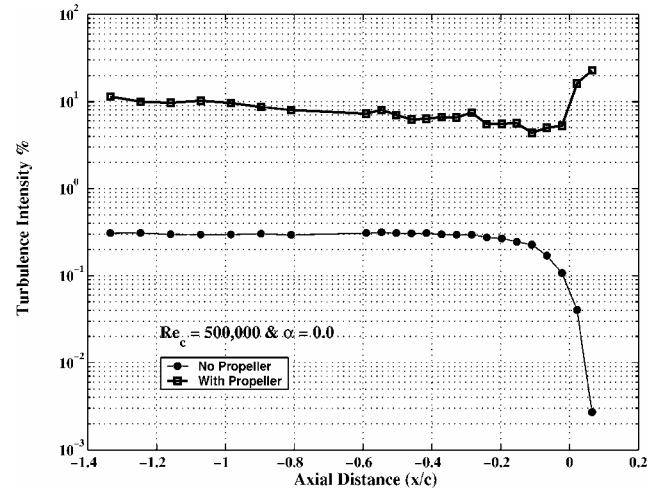

Fig. 12 Centerline turbulence intensity for the two-dimensional inlet—with and without propeller.

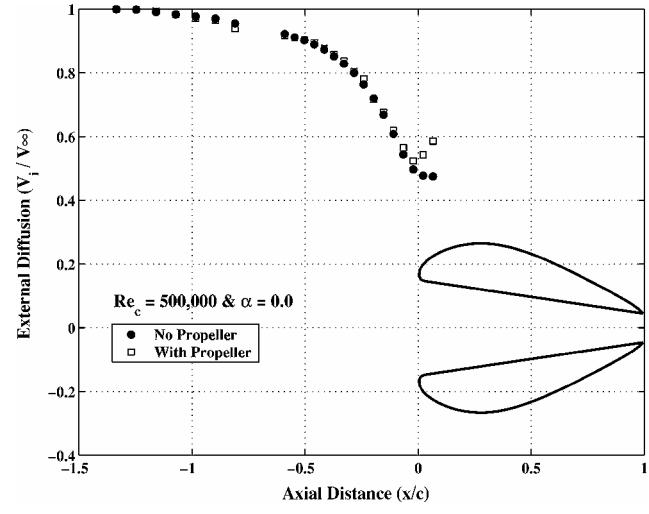

Fig. 13 External diffusion of the two-dimensional inlet—with and without propeller.

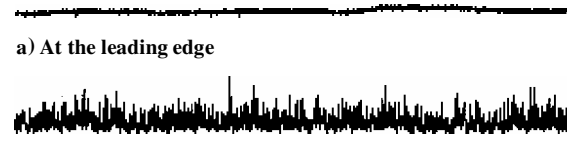

a) At the leading edge

b) At the fin

Fig. 14 Hot-film signals, two-dimensional inlet: $Re_c = 0.5 \times 10^6$—no propeller.

it. However, the natural decay of turbulence is not taken into consideration. Moreover, the mean velocity only changes by a factor of two, as can been seen in Fig. 13, which means that the effective area ratio is small. Introduction of the propeller slipstream, which contains large-scale, organized, and anisotropic structures, elevates the turbulence level from 0.3% with no propeller up to about 9% (averaged over a blade passage cycle). In this case a slight decrease in turbulence intensity along the stream tube is observed, while it appears to increase inside the inlet, as shown in Fig. 13. The slight decrease can be attributed to having faster natural decay than the increase within the stream tube predicted by Prandtl's analysis, resulting in a global slight decay. This faster decay can be attributed to the large-scale structures embedded within the flow via the slipstream, however, the increase in turbulence intensity inside the inlet is contradictory.

The sample vs time traces of the hot-film signals, shown in Fig. 14, show that the flow without slipstream is laminar at the

inlet leading edge and transient at the internal fin. When the propeller slipstream is introduced, the previously transient flow is now partially laminarized by the slipstream, as seen in Fig. 15. The previously laminar flow at the surface becomes transient as indicated by the power spectra shown in Fig. 16, which reveal higher activity over a wider frequency band and also a band of unstable frequencies around 100 Hz. From the corresponding spectra, shown in Figs. 16c and 16d, it can be seen that energy is distributed among the same frequency components as with no propeller but with a higher energy level, thereby enhancing the mixing process inside the inlet.

At the inlet plane of the two-dimensional inlet, to explore the flow conditions at the wall and on the axis hot-film signals at the leading edge and hot-wire signals taken on the axis, for both cases with and without propeller slipstream, are compared. The voltage vs time traces of the hot-wire signals are shown in Fig. 17. The corresponding spectra are shown in Figs. 18a and 18b and compared with those of the hot-film signals (Figs. 18c and 18d), shown in Fig. 15. The spectrum of the hot-wire signal shows that at the centerline the energy is distributed over a wider range of frequencies. Although the energy level is lower at low frequencies (<60 Hz), it is higher than that of the hot-film signal at higher frequencies. Similar behavior is observed in the case with the propeller slipstream (Figs. 18b and 18d). These higher energy levels at the inlet plane, associated with the propeller slipstream, enhance the mixing process. This helps in improving heat transfer and/or lift, drag, or pressure recovery coefficients,[19,20] where eddies of the upstream flow transmit freestream energy to the walls of the two-dimensional inlet.[18]

Uncertainty Analysis

Uncertainty involved in determining the pressure coefficient C_p from pressure data is computed using the methods of Ref. 21, as follows:

$$C_p = (P_s - P_{\text{ref}})/q_\infty \tag{3}$$

The pressure coefficient uncertainty is then

$$U_{C_p} = \left[\left(\frac{\partial C_p}{\partial \Delta P} U_{\Delta P} \right)^2 + \left(\frac{\partial C_p}{\partial \rho_\infty} U_{P_{\text{ref}}} \right)^2 + \left(\frac{\partial C_p}{\partial V_\infty} U_{V_\infty} \right)^2 \right]^{\frac{1}{2}} \tag{4}$$

$$\left.\begin{aligned} \frac{\partial C_p}{\partial \Delta P} &= \frac{1}{\frac{1}{2}\rho_\infty V_\infty^2} = \frac{C_p}{\Delta P} \\ \frac{\partial C_p}{\partial \rho_\infty} &= \frac{-\Delta P}{\frac{1}{2}\rho_\infty^2 V_\infty^2} = \frac{-C_p}{\rho_\infty} \\ \frac{\partial C_p}{\partial V_\infty} &= \frac{-2\Delta P}{\frac{1}{2}\rho_\infty V_\infty^3} = \frac{-2C_p}{V_\infty} \end{aligned}\right\} \tag{5}$$

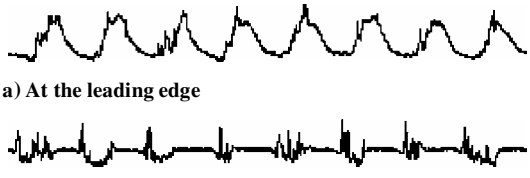

a) At the leading edge

b) At the fin

Fig. 15 Hot-film signals, two-dimensional inlet: $Re_c = 0.5 \times 10^6$— propeller rpm = 240.

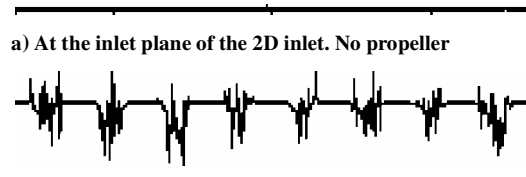

a) At the inlet plane of the 2D inlet. No propeller

b) At the inlet plane of the 2D inlet. Propeller rpm = 240

Fig. 17 Two-dimensional inlet hot-wire signals on the axis of the inlet plane: $Re_c = 0.5 \times 10^6$.

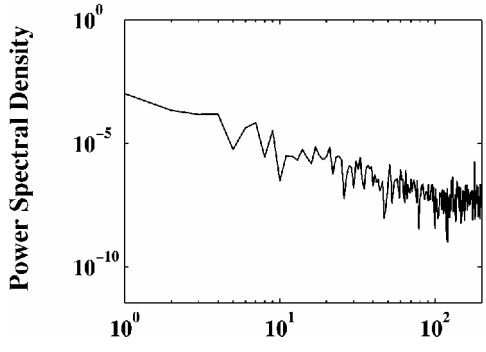

a) No propeller, leading edge

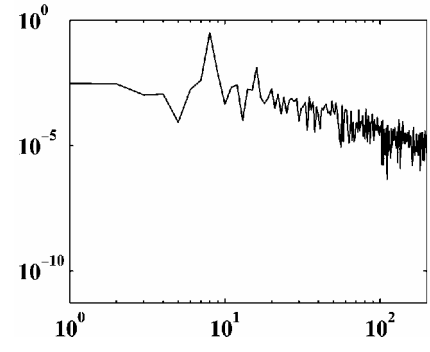

b) With propeller, leading edge

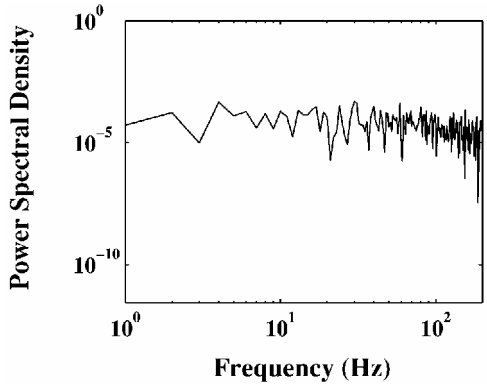

c) No propeller, at the fin

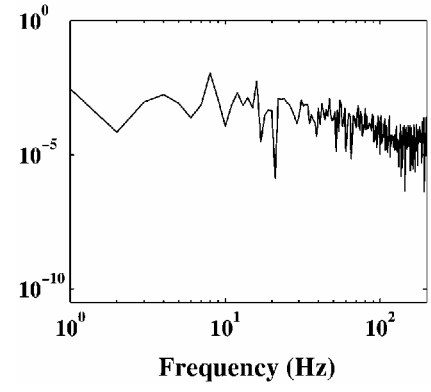

d) With propeller, at the fin

Fig. 16 Hot-film power spectra for the two-dimensional inlet: $Re_c = 0.5 \times 10^6$.

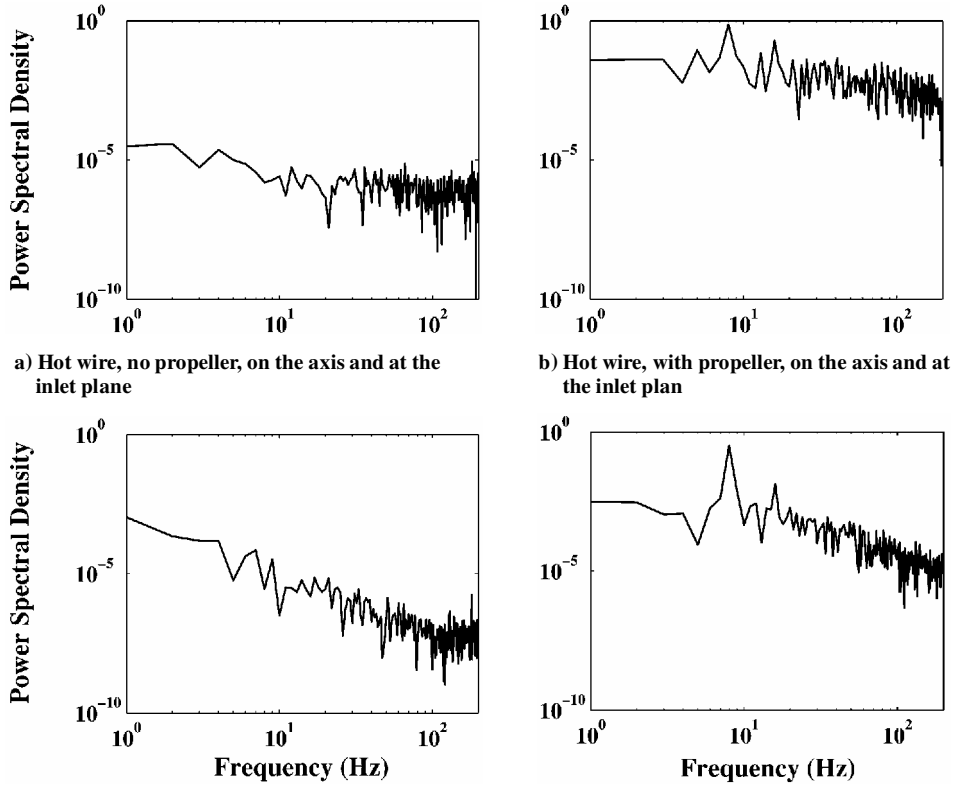

a) Hot wire, no propeller, on the axis and at the inlet plane

b) Hot wire, with propeller, on the axis and at the inlet plan

c) Hot film, no propeller, at the leading edge

d) Hot film, with propeller, at the leading edge

Fig. 18 Two-dimensional inlet power spectra from hot-wire and hot-film signals: $Re_c = 0.5 \times 10^6$.

leading to

$$U_{C_p}/C_p = \left[(U_{\Delta P}/\Delta P)^2 + \left(-U_{\rho_\infty}/\rho_\infty\right)^2 + \left(-2U_{V_\infty}/V_\infty\right)^2\right]^{\frac{1}{2}} \tag{6}$$

Similarly, one can obtain the uncertainties of ρ_∞ and V_∞ as follows:

$$U_{\rho_\infty}/\rho_\infty = \left[\left(U_{P_\infty}/P_\infty\right)^2 + \left(-U_{T_\infty}/T_\infty\right)^2\right]^{\frac{1}{2}} \tag{7}$$

$$U_{V_\infty}/V_\infty = \left[\left(U_{P_\infty}/P_\infty\right)^2 + \left(U_{T_\infty}/2T_\infty\right)^2 + \left(U_{q_\infty}/2q_\infty\right)^2\right]^{\frac{1}{2}} \tag{8}$$

With relative uncertainties of 0.001 and 0.08% for temperature and pressure measurements respectively, the 95% confidence relative uncertainty of the pressure coefficient is

$$U_{C_p}/C_p = 0.21166\%$$

Conclusions

For the two-dimensional inlet-airfoil in the presence of the propeller slipstream and at a chord Reynolds number of 5×10^5, the following is concluded:

1) The slipstream does not significantly affect the lift performance, that is, the pressure distributions. The propeller is unpowered, and the separation bubble is short.

2) The mean transition locations move towards the leading edge by about 10%c, compared to the case without the slipstream. The separation bubble does survive, albeit as a transient phenomena.

For the two-dimensional inlet, with internal fin, at a chord Reynolds number of 5×10^5, the following is concluded:

1) There is no change in the external diffusion of the flow approaching the inlet.

2) With the propeller slipstream, inside the two-dimensional inlet, the flow becomes transitional on the fin instead of being laminar without slipstream. The turbulence intensity distribution shows an increase that starts from the inlet plane of the two-dimensional inlet, reflecting an enhancement of mixing and, consequently, heat-transfer rates that can take place at the heat-exchanger location.

References

[1]Mueller, T. J., "Low Reynolds Number Vehicles," AGARDograph No. 288, Loughton, Essex, UK, Feb. 1985.

[2]Bents, D. J., Mockler, T., Maldonado, J., Hahn, A., Cyrus, J., Schmitz, P., Harp, J., and King, J., "Propulsion Selection for 85kft Remotely Piloted Atmospheric Science Aircraft," NASA TM 107302, 1996.

[3]Drela, M., "Aerodynamics of Heat Exchangers for High-Altitude Aircraft," AIAA Paper-95-1866-CP, 1995.

[4]Martin, P., "The Design and Testing of an Inlet-Airfoil for a High Altitude Remotely Piloted Aircraft," M.S. Thesis, Aerospace Engineering Dept., Old Dominion Univ., Norfolk, VA, May 1998.

[5]Young, A. D., and Moris, D. E., "Note on Flight Tests on the Effect of the Slipstream on Boundary-Layer Flow," British Aeronautical Research Council, R&M No. 1957, London, Sept. 1939.

[6]Young, A. D., and Moris, D. E., "Further Note on Flight Tests on the Effect of the Slipstream on Boundary-Layer Flow," RAM Rept. B. A. 1404b, 1939.

[7]Hood, M. J., and Gaydos, M. E., "Effects of Propellers and Vibration on the Extent of the Laminar Flow on the NACA 27-212 Airfoil," NACA ACR WR L-784, Oct. 1939.

[8]Wenzinger, C. J., "Wind-Tunnel Investigation of Several Factors Affecting the Performance of a High-Speed Pursuit Airplane with Air Cooled Radial Engine," NACA Advance Confidential Report (ACR), Nov. 1941 (Available as 82-N74537).

[9]Zalovcik, J. A., "Flight Investigation of Boundary Layer and Profile-Drag Characteristics of Smooth Wing Sections of a P-47D Airplane," NACA WR L-86 (Formerly ACR No. L5H11a), Oct. 1945.

[10]Zalovcik, J. A., and Skoog, R. B., "Flight Investigation of Boundary Layer Transition and Profile-Drag of an Experimental Low-Drag Wing Installed on a Fighter Type Airplane," NACA WR L-94, 1945.

[11]Holmes, B. J., Obara, C. J., and Yip, L. P., "Natural Laminar Flow Experiments on Modern Aerodynamic Surfaces," NASA TP-2256, June 1984.

[12]Küchemann, D., and Weber, J., *Aerodynamics of Propulsion*, McGraw–Hill, New York, 1953, Chap. 4.

[13]Elsaadawy, E., and Britcher, C. P., "Experimental Investigation of the Effects of Propeller Slipstream on the Behavior of Boundary Layers at Low Reynolds Number," AIAA Paper 2000-4123, Aug. 2000.

[14]Elsaadawy, E., "Experimental Investigation of the Effects of Propeller Slipstream on the Behavior of Boundary Layers at Low Reynolds Number," Ph.D. Dissertation, Dept. of Aerospace Engineering, Old Dominion Univ., Norfolk, VA, Dec. 2001.

[15]Coskun, O., "The Design and Testing of a 2D Inlet for a High Altitude, Low Speed, Remotely Piloted Aircraft," Aerospace Engineering Dept., Old Dominion Univ., Internal Report, Norfolk, VA, May 1999.

[16]Bruun, H. H., *Hot-Wire Anemometry: Principles and Signal Analysis*, Oxford Univ. Press, Oxford, 1995, Chap. 8.

[17]Johnson, C. B., Carraway, D. L., Stainback, and Fancher, M. F., "Hot-Film System for Transition Detection in Cryogenic Wind Tunnels," NASA CP 2487 (Part 2), March 1987.

[18]Hoffmann, J. A., and Gonzalez, G., "Effects of Small-Scale, High Intensity Inlet Turbulence on Flow in a Two-Dimensional Diffuser," *Journal of Fluids Engineering*, Vol. 106, June 1984, pp. 121–124.

[19]Sharan, V. K., "Improving Diffuser Performance by Artificial Means," *AIAA Journal*, Vol. 10, Aug. 1972, pp. 1105, 1106.

[20]Hoffmann, J. A., "Effect of Free-Stream Turbulence on Diffuser Performance," *Journal of Fluids Engineering*, Vol. 103, Sept. 1981, pp. 385–390.

[21]Kline, S. J., and McClintock, F. A., "Describing Uncertainties in Single-Sample Experiments," *Mechanical Engineering*, Vol. 75, No. 1, 1953, pp. 3–5.